Electronic Supplementary Information

Pillar[5]arene-Based Crosslinked Polymer Gel Films for Organic Dyes Adsorption

Changjun Gan[a], Liping Zhu[a] and Wenzhong Huang[a*]

[a]School of Chemistry and Chemical Engineering, Kunming University, Kunming, 650214, People's Republic of China

E-mail: Huangwz@kmu.edu.cn

1. Synthesis of Compounds

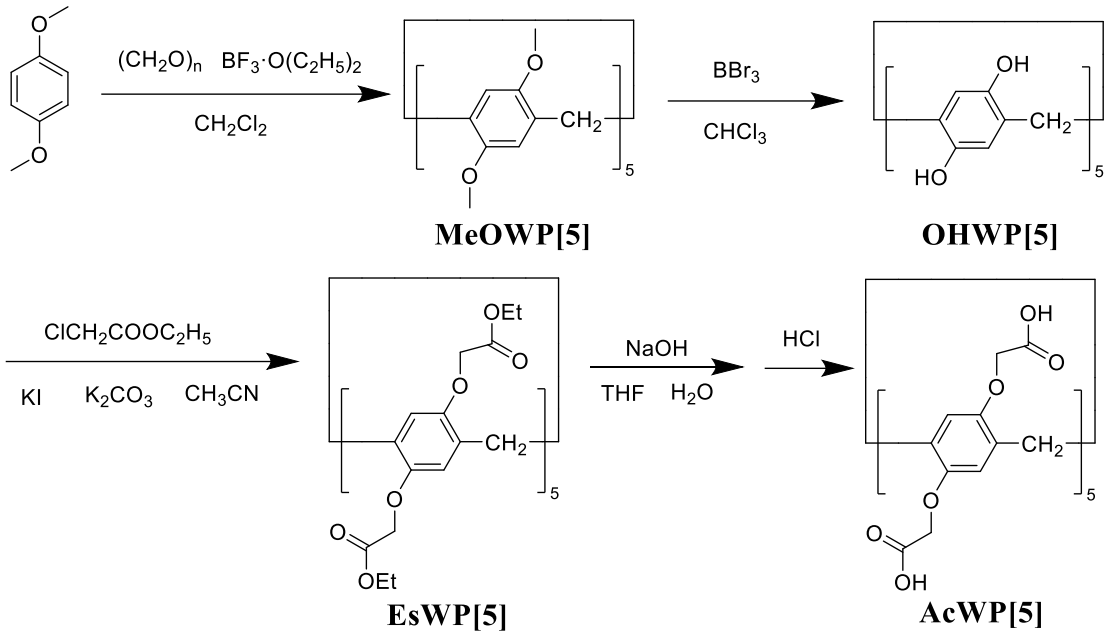

Figure S1: Synthetic route of WP5[1–4,16]

Synthesis of compound MeOWP[5]:

In a round-bottom flask, 1,4-dimethoxybenzene (4.14 g, 29.96 mmol), paraformaldehyde (0.99 g, 32.97 mmol), dichloromethane (240 mL), and boron trifluoride diethyl etherate (5.52 g, 38.89 mmol) were sequentially added. The reaction mixture was stirred at room temperature for 6 h. Subsequently, aqueous acid was added to quench the reaction, and the resulting mixture was stirred for an additional 2 h. The suspension was then filtered, and the filtrate was concentrated under reduced pressure to afford the crude product. Purification by silica gel column chromatography (petroleum ether/ethyl acetate = 10:1, v/v) yielded the title compound MeOWP[5] as a white solid (55.64% yield). ^{1}H NMR(400 MHz, $CDCl_3$): δ(ppm) 6.76 (s, 10 H), 3.78(s, 10H), 3. 64 (s, 30H). ^{13}C NMR (100 MHz, $CDCl_3$): δ(ppm): 150.9, 128.3, 114.2, 55.9, 29.8.

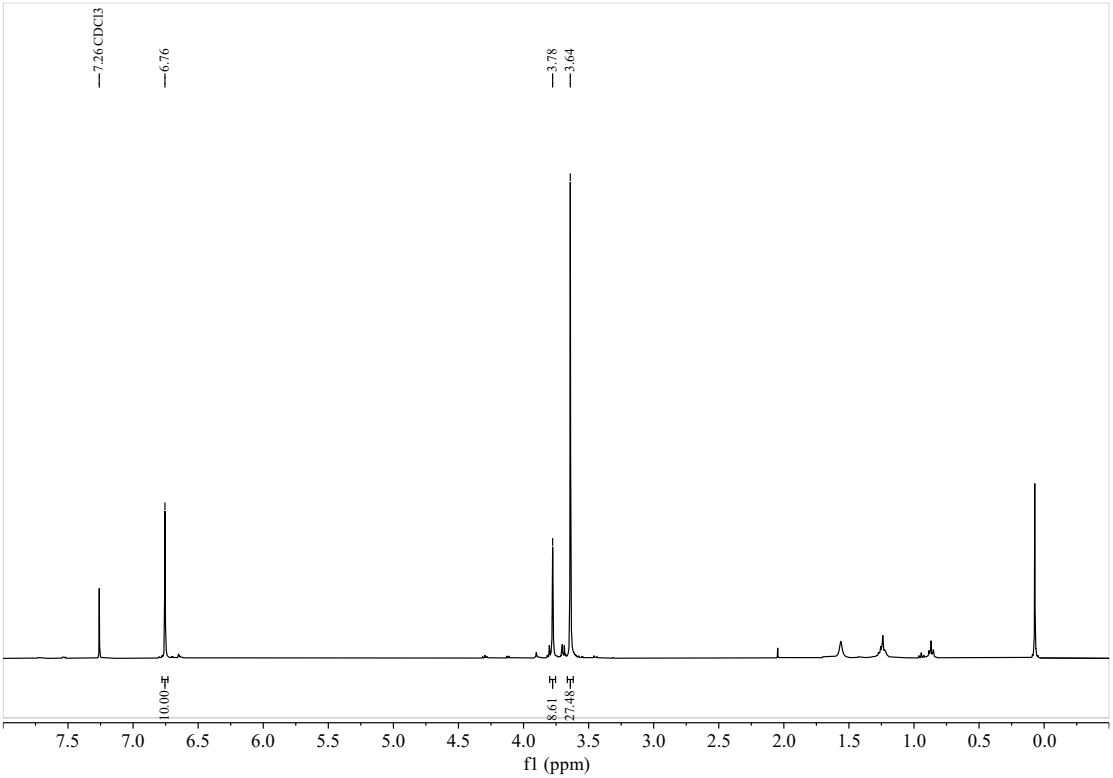

Figure S2: ^{1}H NMR spectrum(400 MHz, $CDCl_3$, rt) of **MeOWP[5]**

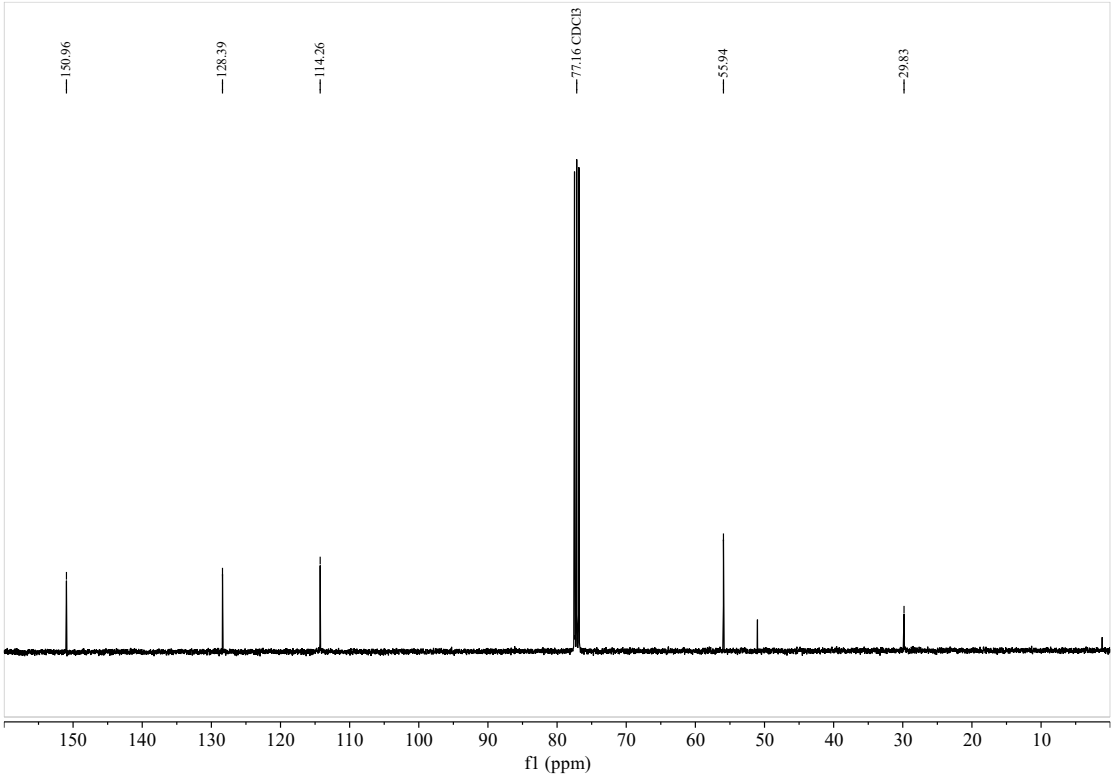

Figure S3: ^{13}C NMR spectrum (100 MHz, $CDCl_3$, rt) of **MeOWP[5]**

Synthesis of compound OHWP[5]:

To a round-bottom flask was added MeOWP[5] (1.00 g, 1.33 mmol) dissolved in chloroform (100 mL), followed by the addition of boron tribromide (6.68 g, 26.67 mmol). The reaction mixture was stirred at room temperature for 48 h. Upon completion, water (50 mL) was added, and stirring was continued for an additional 2 h. The resulting suspension was collected by vacuum filtration. The solid residue was washed sequentially with acidic aqueous solution and diethyl ether, then lyophilized to afford OHWP[5] as a white powder in 98.31% yield. ^{1}H NMR (400 MHz, DMSO-d$_6$) δ(ppm): 8.45 (s, 10H), 6.57(s, 10H), 3.40(s, 10H). ^{13}C NMR (100 MHz, DMSO-d$_6$): δ(ppm): 146.1, 126.4, 117.3, 64.9, 29.1.

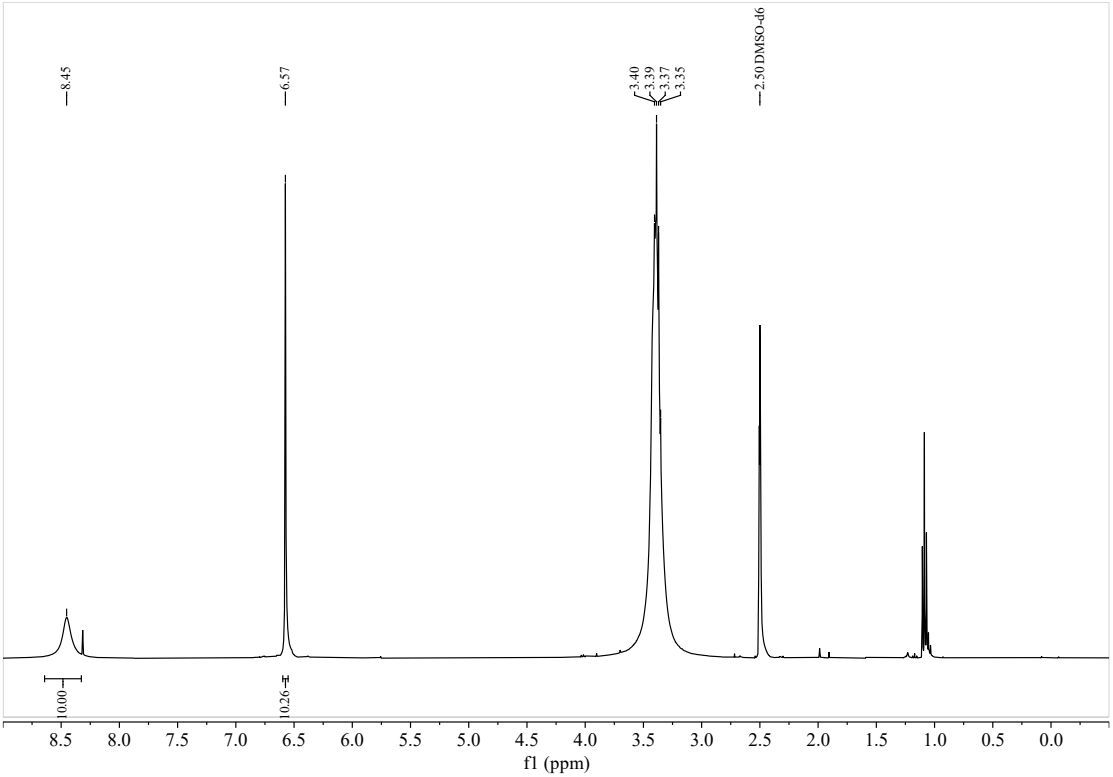

Figure S4: ^{1}H NMR spectrum (400 MHz, DMSO-d$_6$, rt) of **OHWP[5]**

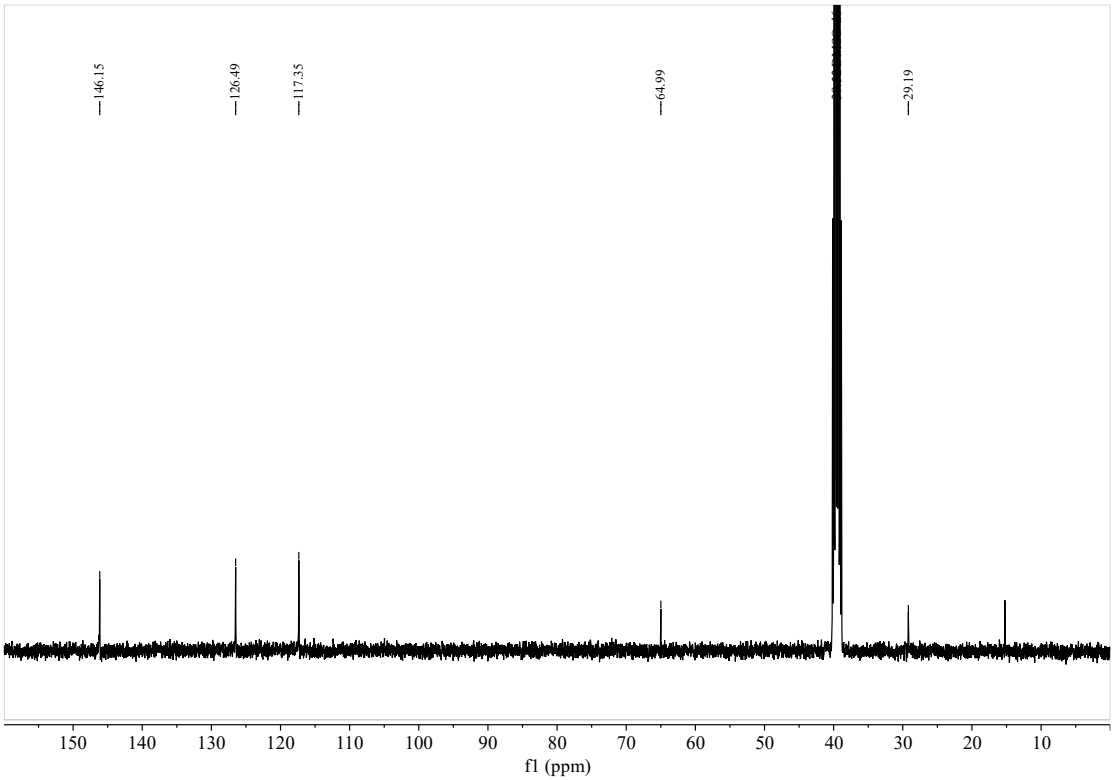

Figure S5: ^{13}C NMR spectrum (100 MHz, DMSO-d_6, rt) of **OHWP[5]**

Synthesis of compound EsWP[5]:

To a round-bottom flask were added OHWP[5] (0.25 g, 0.40 mmol), anhydrous potassium carbonate (0.69 g, 4.99 mmol), and acetonitrile (18 mL). The mixture was stirred at room temperature for 0.5 h, followed by the addition of potassium iodide (0.07 g, 0.42 mmol) and ethyl chloroacetate (1.02 mL, 9.57 mmol). The reaction mixture was then heated to reflux at 80 °C for 18 h. After cooling to room temperature, the mixture was diluted with water and extracted with chloroform. The combined organic layers were concentrated under reduced pressure, and the residue was treated with a minimal amount of methanol. The resulting precipitate was collected by vacuum filtration to afford EsWP[5] as a white solid in 66.67% yield. ^{1}H NMR (400MHz, $CDCl_3$,) δ(ppm):7.04(s, 10H), 4.54(d, J = 8.0 Hz, 20H), 4.16–3.99(m, 20H), 3.85(s, 10H), 0.96(t, J=7.2 Hz, 30H). ^{13}C NMR (100 MHz, $CDCl_3$): δ(ppm): 169.5, 149.1, 128.8, 114.6, 65.8, 61.0, 29.8, 13.9.

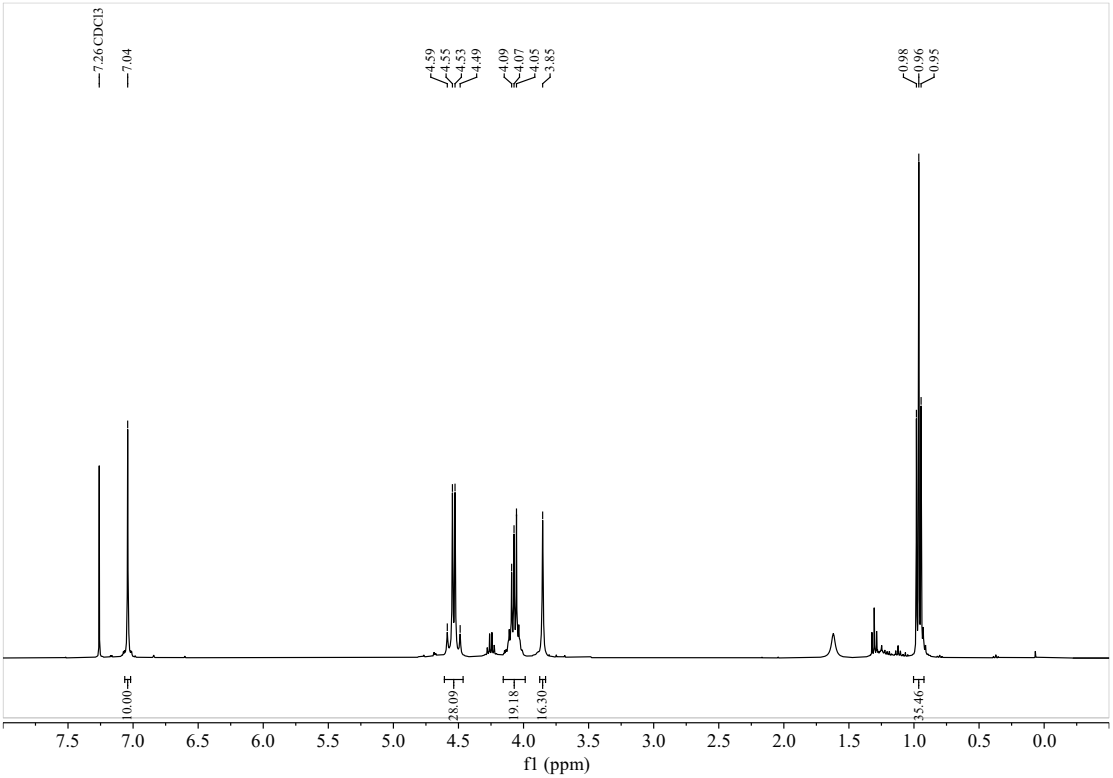

Figure S6: ^{1}H NMR spectrum (400 MHz, $CDCl_3$, rt) of **EsWP[5]**

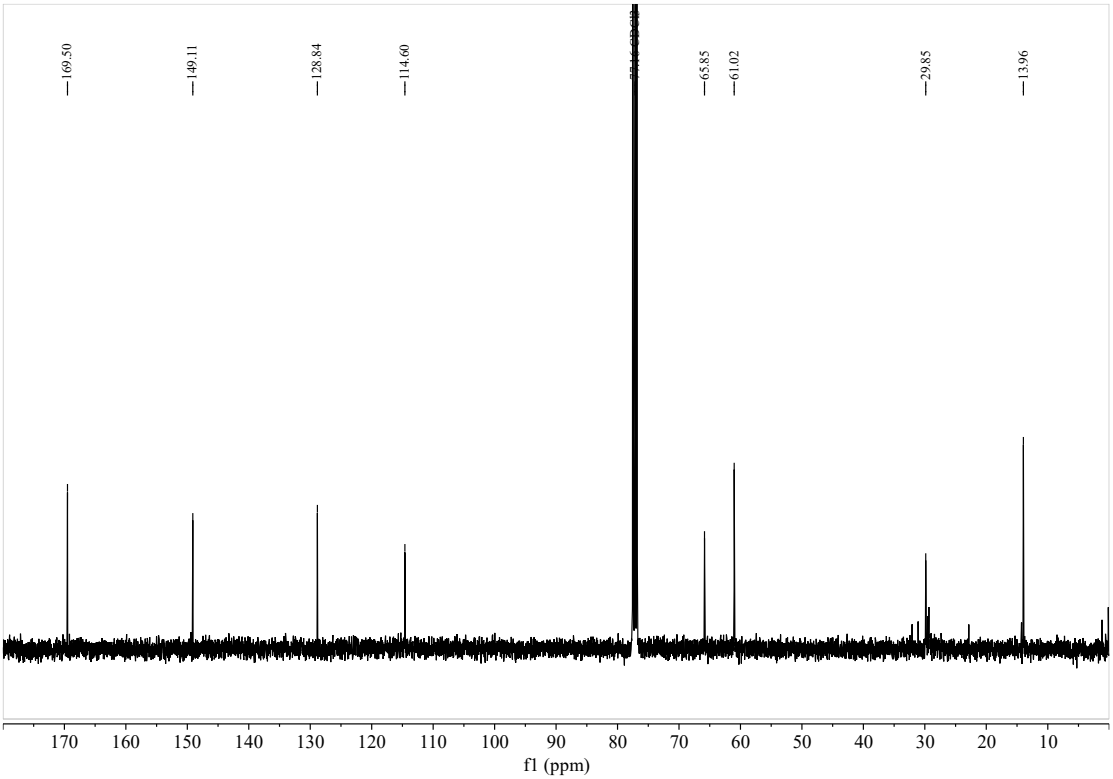

Figure S7: ^{13}C NMR spectrum (100 MHz, $CDCl_3$, rt) of **EsWP[5]**

Synthesis of compound AsWP[5]:

EsWP[5] (0.34 g, 0.23 mmol) was dissolved in tetrahydrofuran (THF, 19 mL), followed by the addition of sodium hydroxide (2.77 g, 69.25 mmol) and distilled water (24 mL). The resulting mixture was heated to reflux at 90 °C for 15 h. After cooling to room temperature, THF was removed under reduced pressure. The aqueous residue was diluted with water and acidified with concentrated hydrochloric acid to pH 2–3. The precipitated solid was collected by filtration, washed with water, and dried to afford AsWP[5] as a pale yellow powder in 91.44% yield. ^{1}H NMR (400MHz, DMSO-d$_6$) δ(ppm):12.94(s, 10H), 7.11(s, 10H), 4.71(d, J=15.9 Hz, 10H), 4.43(d, J=15.8 Hz, 10H), 3.74(s, 10H). ^{13}C NMR (100 MHz, DMSO-d$_6$): δ(ppm): 170.5, 148.4, 128.0, 114.2, 65.0.

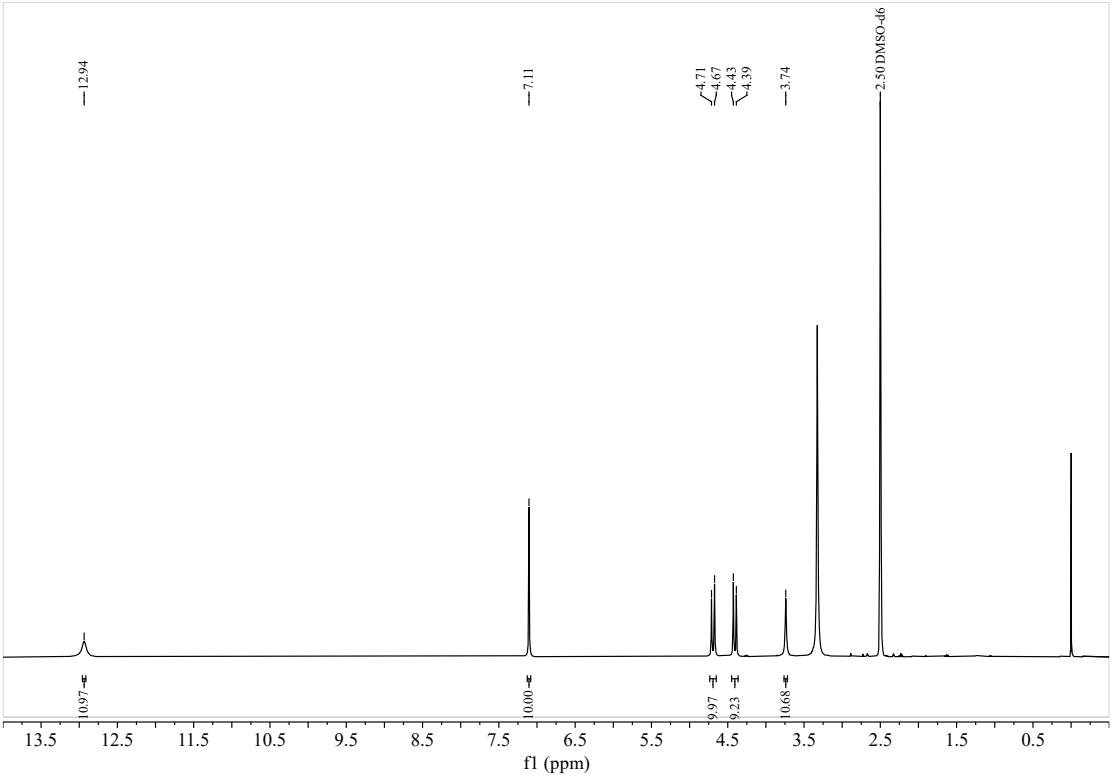

Figure S8: ^{1}H NMR spectrum(400 MHz, DMSO-d$_6$, rt) of **AsWP[5]**

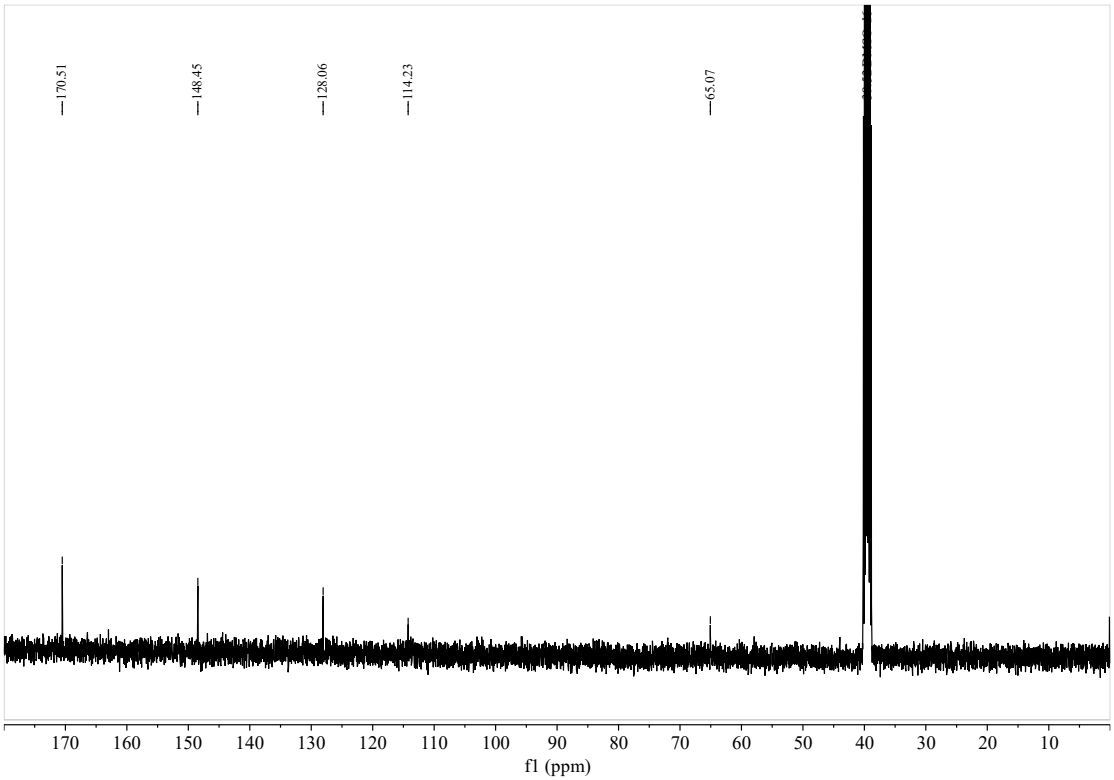

Figure S9: ^{13}C NMR spectrum(100 MHz, DMSO-d$_6$, rt) of **AsWP[5]**

2. Adsorption of dyes

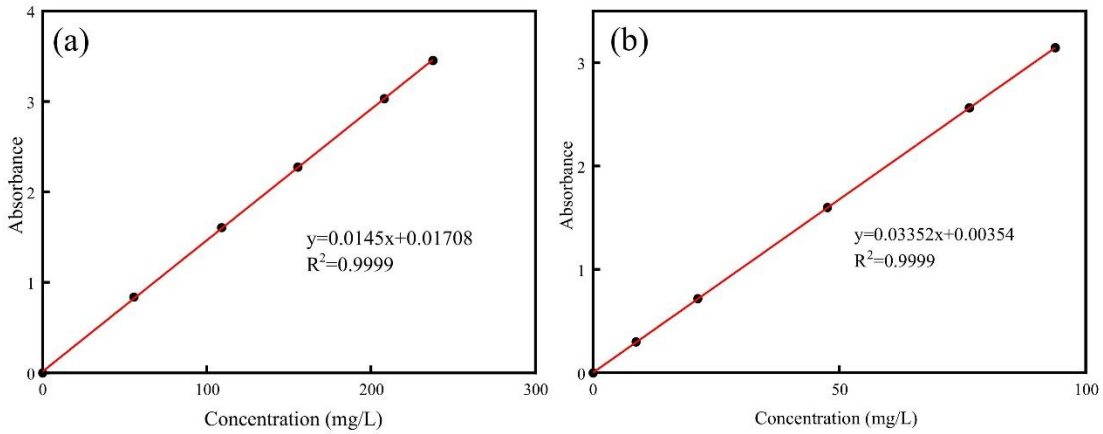

Figure S10: (a) The standard curve of RhB; (b) The standard curve of BR46.

3. Investigation of the Adsorption Mechanism

Fig 10 presents the ^{1}H NMR spectra of carboxylated pillar[5]arene, rhodamine B, and the precipitate formed upon mixing carboxylated pillar[5]arene with rhodamine B. Comparison of the spectra reveals that the ^{1}H NMR signals of the pillar[5]arene remain virtually unchanged before and after exposure to rhodamine B, indicating the absence of a host–guest interaction between carboxylated pillar[5]arene and rhodamine B under

the experimental conditions employed.

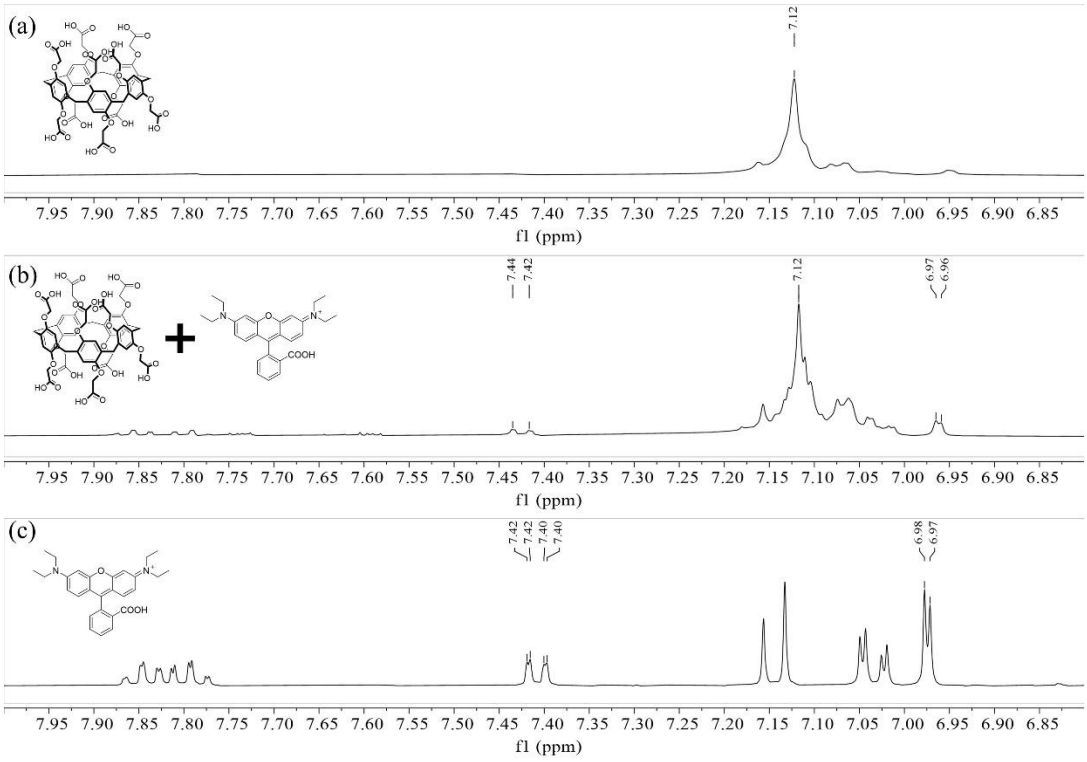

Figure S11: ^{1}H NMR (400MHz, CD3OD, 293K) of (a) AsWP[5]; (b) AsWP[5]⊃RhB; (c) RhB.

4. Materials Characterization

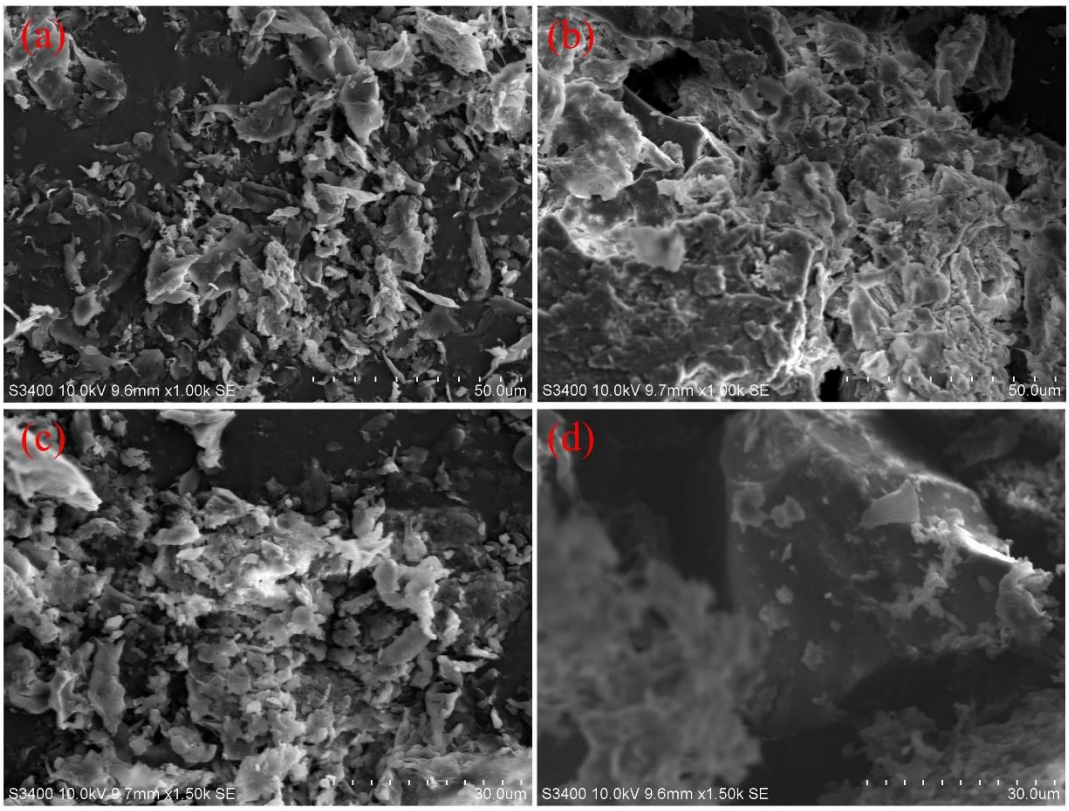

Figure S12: Scanning electron microscopy (SEM) images of: (a) PVA–AA–WP[5] after RhB adsorption; (b) VA–AA–WP[5] after BR46 adsorption; (c) PVA–WP[5] after RhB adsorption; (d) PVA–WP[5] after BR46 adsorption.

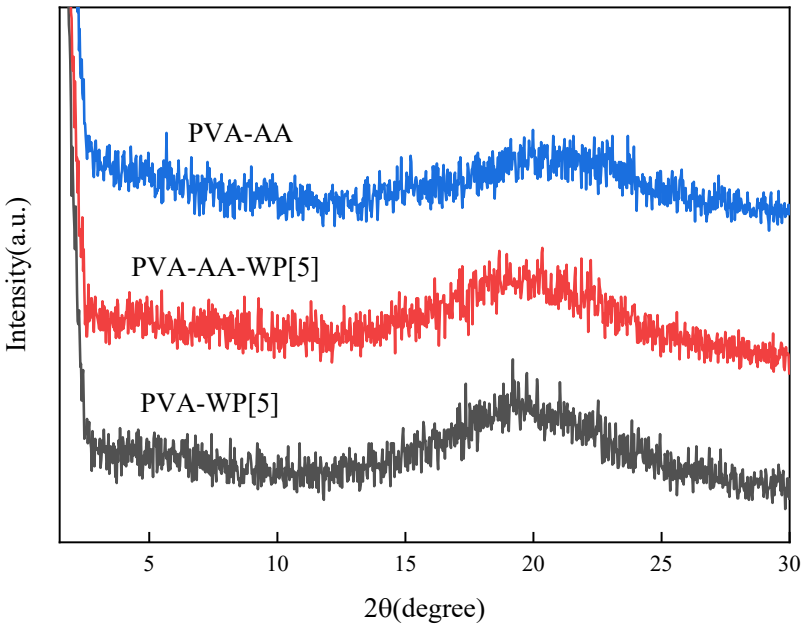

Figure S13: PXRD Patterns of PVA-AA, PVA-AA-WP[5], and PVA-WP[5]

5. Dye adsorption

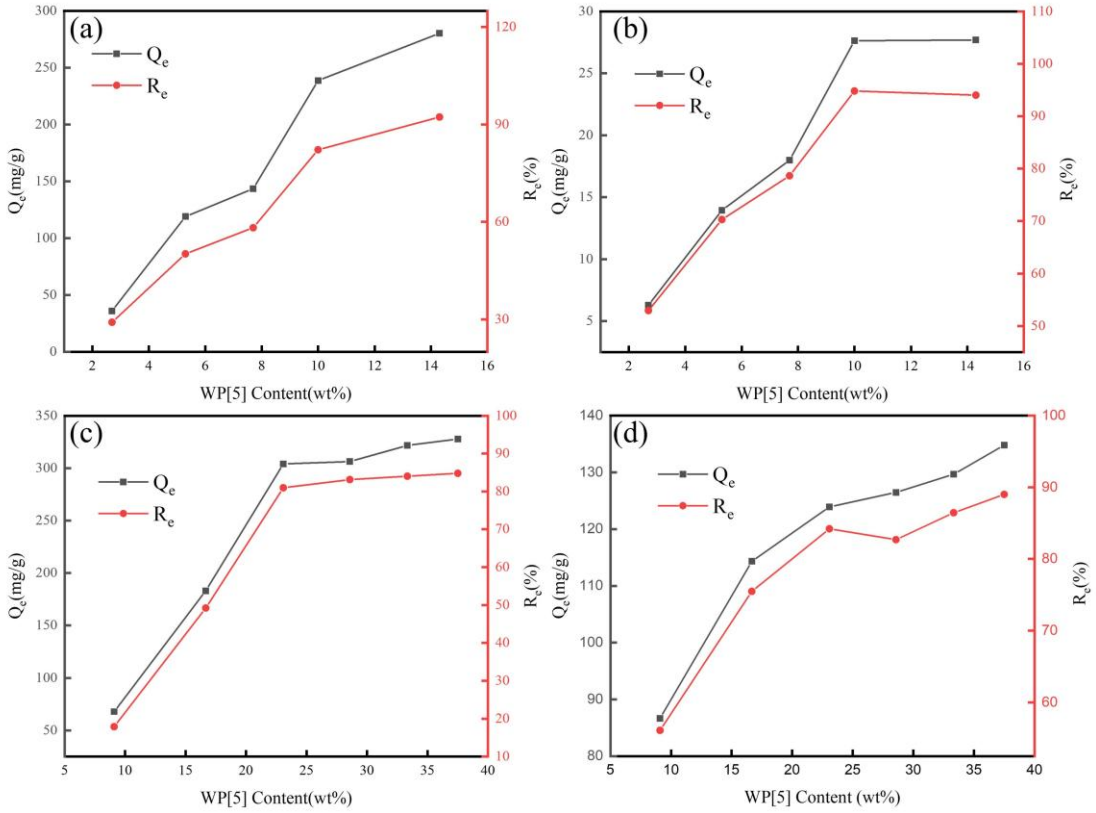

Figure S14: Effect of varying WP[5] content on dye adsorption: (a) adsorption of Rhodamine B (RhB) by HF-1; (b) adsorption of Basic Red 46 (BR46) by HF-1; (c) adsorption of RhB by HF-2; (d) adsorption of BR46 by HF-2.

Table S1. Adsorption of mixed dyes by gel films

No.	Sample	C_0(mg/mL)		C_e(mg/mL)		R_e(%)	
		RhB	BR46	RhB	BR46	RhB	BR46
1	HF-1⊃RhB	0.131	-	0.00160	-	98.8	-
2	HF-1⊃BR46	-	0.0249	-	0.00203	-	91.9
3	HF-1⊃RhB-BR46	0.131	0.0249	0.00657	0.00376	95.3	84.9
4	HF-2⊃RhB	0.131	-	0.000160	-	99.9	-
5	HF-2⊃BR46	-	0.0125	-	0.000410	-	96.7
6	HF-2⊃RhB-BR46	0.131	0.0125	0.00258	0.00133	98.0	89.3

Table S2. Kinetic Parameters of the Adsorption Models

		Pseudo-first-order			Pseudo-second-order		
		K_1,1/min	Q_e,mg/g	R^2	K_2,mg·min/g	Q_e,mg/g	R^2
HF-1	RhB	0.00782	50.8	0.9799	0.000312	197	0.9999
	BR46	0.00762	11.3	0.9356	0.00120	41.7	0.9997
HF-2	RhB	0.0162	310	0.9453	0.0000554	433	0.9925
	BR46	0.0151	32.1	0.8030	0.000561	157	0.9991

[a]Symbols: K_1 and K_2 represent the rate constants of the pseudo-first-order and pseudo-second-order kinetic models, respectively; Q_e denotes the adsorption capacity at equilibrium; R^2 is the correlation coefficient.

Table S3. Parameters of the Adsorption Isotherm Models

	Model	Parameter	RhB	BR46
HF-1	Langmuir	Q_{max}(mg/g)	380	75.1
		K_L(L/mg)	0.00870	0.131
		R^2	0.8155	0.9189
	Freundlich	K_F(L/mg)	2509	282
		n	2.67	1.96
		R^2	0.9187	0.9948
HF-2	Langmuir	Q_{max}(mg/g)	472	226
		K_L(L/mg)	0.0294	0.0805
		R^2	0.9843	0.9631
	Freundlich	K_F(L/mg)	63.3	33.9
		n	2.96	2.29
		R^2	0.9875	0.9946

[a]Symbols: Q_{max}(mg/g): theoretical maximum adsorption capacity; K_L(L/mg): Langmuir constant related to the affinity of binding sites for the dye; K_F(L/mg): Freundlich constant indicative of adsorption capacity; n: Freundlich exponent reflecting adsorption intensity or surface heterogeneity.

Table S4. Comparison of Rhodamine B (RhB) Adsorption Capacities Among Different Adsorbents.

Sr. No.	Adsorbent materials	Q_e(mg/g)	Reference
1	Lotus leaf porous carbon	718	[5]
2	NiO/AC active electrode	168	[6]
3	Plantain peel activated biochar	84.4	[7]
4	Chitosan-based polyurethane foams	48.4	[8]
5	MOF-5@GO nanocomposites	151	[9]
6	Carbon graphite/CNT composites	0.437	[10]
7	New collagen-based cryogel	120	[11]
8	Graphene oxide/polydopamine adsorptive membrane	87.0	[12]
9	Nitrogen-enriched magnetic porous carbon	137	[13]
10	TCM residue biochar	309	[14]
11	Mg–Al LDH@EDTA-Melamine nanocomposite	232	[15]
12	Pillararene gel thin film	448	This work

References

1 G. Xu, P. Yang, Y. Zhang, L. Sun, X. Hu, W. Zhang, Y. Tu, Y. Tian, A. Li, X. Xie and X. Gu, *Chemosphere*, 2023, **341**, 140056.

2 W.-Q. Gong, Y.-X. Fu, Y. Zhou, M.-S. Sun, Z.-M. Li, N.-H. Lu and D.-J. Tao, *Sep. Purif. Technol.*, 2023, **322**, 124304.

3 Q. Yao, B. Lü, C. Ji, Y. Cai and M. Yin, *ACS Appl. Mater. Interfaces*, 2017, **9**, 36320–36326.

4 L. Gao, T. Wang, K. Jia, X. Wu, C. Yao, W. Shao, D. Zhang, X.-Y. Hu and L. Wang, *Chem. - Eur. J.*, 2017, **23**, 6605–6614.

5 A. Li, W. Huang, N. Qiu, F. Mou and F. Wang, *Mater. Res. Express*, 2020, **7**, 55505.

6 A. Chennah, M. A. Khan, M. Zbair and H. Ait Ahsaine, *Catalysts*, 2023, **13**, 1009.

7 F. A. Adekola, S. B. Ayodele and A. A. Inyinbor, *Chem. Data Collect.*, 2019, **19**, 100170.

8 T. Boominathan, I. Singh, J. S. Krishna, S. Perinbanathan, S. M. Arbaaz, S. Latha, S. Karthikeyan, R. Desikan, C. V. S. B. Rao and A. Sivaramakrishna, *Int. J. Biol. Macromol.*, 2024, **279**, 134999.

9 G. Kumar and D. T. Masram, *ACS Omega*, 2021, **6**, 9587–9599.

10 S. Zghal, I. Jedidi, M. Cretin, S. Cerneaux and M. Abdelmouleh, *Materials*, 2023, **16**, 1015.

11 S. Azadi, M. Esmkhani and S. Javanshir, *J. Sol-Gel Sci. Technol.*, 2022, **103**, 405–415.

12 X. Wang, Y. Guo, Z. Jia, H. Ma, C. Liu, Z. Liu, Q. Shi, B. Ren, L. Li, X. Zhang and Y. Hu, *Desalination*, 2021, **516**, 115220.

13 J. Zhang, X. Hu, X. Yan, R. Feng, M. Zhou and J. Xue, *Colloids Surf., A*, 2019, **575**, 10–17.

14 P. Li, T. Zhao, Z. Zhao, H. Tang, W. Feng and Z. Zhang, *ACS Omega*, 2023, **8**, 4813–4825.

15 M. Ara and H. Ghafuri, *Heliyon*, 2024, **10**, e32447.

16 T. Ogoshi, M. Hashizume, T. Yamagishi and Y. Nakamoto, *Chem. Commun.*, 2010, **46**, 3708.